Eur. J. Mineral.
2006, **18**, 379–391

Ti-rich phlogopite from Mt. Vulture (Potenza, Italy) investigated by a multianalytical approach: substitutional mechanisms and orientation of the OH dipoles

FERNANDO SCORDARI[1]*, GENNARO VENTRUTI[1], ANNA SABATO[1], FABIO BELLATRECCIA[2], GIANCARLO DELLA VENTURA[2] and GIUSEPPE PEDRAZZI[3]

[1]Dipartimento Geomineralogico, Università di Bari, via E. Orabona 4, I-70125 Bari, Italy
*Corresponding author, e-mail: f.scordari@geomin.uniba.it
[2]Dipartimento di Scienze Geologiche, Università di Roma Tre, Largo S. Leonardo Murialdo 1, I-00146 Roma, Italy
[3] Dipartimento di Sanità Pubblica, Sezione di Fisica, Plesso Biotecnologico Integrato, via Volturno 39, I-43100 Parma, Italy

Abstract: Trioctahedral mica samples, collected at Cava St. Antonio (Mt. Vulture, Italy) were studied by combining electron-microprobe and C-H-N elemental analyses, single-crystal X-ray diffraction refinement, Mössbauer and Fourier transform infrared spectroscopies.

Electron-microprobe analyses show the crystals to be quite homogeneous with TiO_2 ~3 wt % and F ranging from 0.42 to 0.59 wt %. Quantitative analyses of H combined with ferric/ferrous ratios from Mössbauer data allowed reliable crystal-chemical formulae to be derived. The results suggest that the entry of both Ti^{4+} and Fe^{3+} in the structure occurs through R-oxy substitution mechanisms involving deprotonation at O(4). This inference is supported by X-ray structure-refinement results (notably the *c* cell-parameter, the off-centering of the M2 cation towards O(4), the bond-length distortions of the *cis*-M2 octahedron) obtained using anisotropic thermal parameters in space group *C*2/*m*. The amount of oxy-substitutions from both electron-microprobe and X-ray data is in agreement with carbon-hydrogen-nitrogen analyses which give an average anion composition ($OH_{1.25}O_{0.65}F_{0.10}$).

Polarized-light infrared spectroscopy shows a complex OH-stretching spectrum which is composed of several overlapping (at least five) components. These can be assigned to the main octahedral local configurations that are compatible with the chemical composition. Pleochroic Fourier transform infrared spectroscopy measurements done along the principal optical directions show that the O-H bond axis is tilted from [001] and provide the average orientation of the O-H dipole in the structure: O-H ^ $\alpha \sim 23°$ and O-H ^ $\gamma \sim 56°$.

Key-words: trioctahedral 1*M*-micas bearing titanium, crystal chemistry, EMPA, C-H-N elemental analysis, SREF, Mössbauer, polarized-light FTIR.

Introduction

Trioctahedral micas are common minerals of igneous and metamorphic rocks formed over a wide range of geological environments and under different chemical and physical conditions. Their compositional variation and cation arrangement in fact depends strongly on the intensive parameters (temperature, pressure, fH_2O and fO_2) during crystallization. The relationship between cation substitutions/orderings and the structural parameters has been addressed in a large number of studies (Weiss *et al*., 1985; Brigatti & Guggenheim, 2002 and references therein). However, the quantitative OH direct determination and estimate of the valence state and structural role of transition metals, such as Ti and Fe, to obtain a reliable crystal-chemical, or structural formula for these minerals (Dyar *et al*., 1993; Virgo & Popp, 2000; Righter *et al*., 2002; Cesare *et al*., 2003; Schingaro *et al*., 2005) have been rarely addressed. These points are of paramount importance when using the crystal-chemical data of micas to model the geological conditions of formation of the host rock.

The aim of the present study is a detailed characterization of a series of Ti-bearing trioctahedral micas from a pyroclastic level outcropping at Cava St. Antonio (Mt. Vulture, Potenza, Italy). Our approach combines crystal-structure refinement (SREF = Structure REFinement), electron-microprobe analysis (EMPA), C-H-N microelemental analysis for H, Mössbauer spectroscopy for Fe^{3+}/Fe^{2+} analysis, and Fourier transform infrared (FTIR) spectroscopy on single crystal by polarized light to characterize the local structural environments and the orientation of the O-H dipoles in the structure.

DOI: 10.1127/0935-1221/2006/0018-0379
0935-1221/06/0018-0379 $ 5.85

Samples and methods

The mica crystals examined in this paper were collected within the pyroclastic deposits belonging to the third volcano-stratigraphic-unit (VSU) of Mt. Vulture (Caggianelli *et al*., 1990), with a phoiditic-tephritic composition, outcropping at Cava St. Antonio. Five crystals, labelled SA1, were investigated in order to check the homogeneity of the studied mica within the sampled volcanic unit. Each of the five selected crystals was individually studied by SREF and EMPA, while C-H-N and Mössbauer data, used to estimate the OH content and the FeO/Fe_2O_3 ratio, were obtained on a bulk sample.

Chemical composition

Electron-microprobe analyses (Table 1) were obtained from the same crystals used for X-ray intensities collection by means of a Cameca SX-50 electron microprobe operated at 15 kV accelerating voltage, 15 nA sample current with a spot size of 10 μm. The analyses were carried out in WDS mode for F, Na, K, Ba, Cl, Ti, Ca and EDS mode for Si, Al, Mg, Fe. The used standards were: jadeite (Na), periclase (Mg), wollastonite (Si and Ca), rutile (Ti), corundum (Al), magnetite (Fe), orthoclase (K), barite (Ba), fluor-phlogopite (F), sylvite (Cl). Acquisition was done following the procedure of Foley (1989); data reduction was done by the PAP method (Pouchou & Pichoir, 1985).

Determination of H content (Table 1) was performed by bulk C-H-N elemental analysis using the EA 1108 elemental analyzer of CE Instruments at CNR-IGG, Padova, calibrated with standard Acetanilide (C_8H_9NO). The analysis was performed on 40 mg of powdered sample.

Single-crystal intensity data collection

Single-crystal X-ray data collection was performed by means of a Bruker AXS X8 APEX automated diffractometer equipped with a four-circle Kappa goniometer and a CCD detector with a maximum active area diameter of 90 mm, under monochromatized Mo$K\alpha$ radiation with 512 x 512 pixels resolution. The Miracol fibre optics capillary collimator (0.3 mm size) was used to enhance the intensity of the Mo$K\alpha$ radiation and to reduce X-ray beam divergence. Three sets of 12 frames were used for the initial unit-cell determination, each frame measured with 0.5° phi rotation and 10 s exposure time. The crystal-to-detector distance was 40 mm and the collection strategy was optimized by the Apex program suite (Bruker, 2001). Several ω and ϕ rotation sets were used for data collection with 0.5° scan width and at least 10 s per frame exposure time (see Table 3). The package SAINT-IRIX (Bruker, 2003) was employed for data reduction and unit-cell refinement. A semi-empirical absorption correction based on the intensities of equivalent reflections was applied by means the SADABS software (Sheldrick, 2003), and the data were corrected for Lorentz, polarization and background effects.

Mössbauer spectroscopy

Transition ^{57}Fe Mössbauer spectra were recorded at room temperature using a conventional Mössbauer apparatus in transmission geometry with a $^{57}Co/Rh$ single line thin source (~1 GBq). The spectrometer operated in constant acceleration mode with a symmetric triangular velocity shape and a multi-channel analyser with 1024 channels. The velocity range was ±6 mm/s and the velocity was calibrated against sodium-nitroprusside and α-Fe.

Table 1. Average microprobe analyses. Standard deviations are given in parentheses.

	SA1-3	SA1-5	SA1-9	SA1-51	SA1-52
wt%	Mean	Mean	Mean	Mean	Mean
SiO_2	35.77 (0.15)	35.43 (0.12)	37.22(0.12)	35.56 (0.13)	35.58 (0.08)
TiO_2	3.25 (0.06)	3.27 (0.11)	3.25(0.04)	3.63 (0.07)	3.12 (0.01)
Al_2O_3	16.04 (0.10)	16.19 (0.07)	16.42(0.08)	15.53 (0.16)	16.15 (0.14)
Cr_2O_3	0.05 (0.03)	0.03 (0.02)	0.02(0.02)	0.02 (0.02)	0.01 (0.01)
FeO_{tot}	10.24 (0.18)	10.44 (0.07)	11.05(0.12)	11.94 (0.13)	9.90 (0.09)
MnO	0.14 (0.06)	0.15 (0.05)	0.18(0.03)	0.19 (0.05)	0.17 (0.01)
MgO	17.41 (0.14)	17.54 (0.15)	17.82(0.09)	16.92 (0.13)	17.51 (0.11)
BaO	1.80 (0.09)	2.13 (0.14)	1.04(0.04)	1.73 (0.17)	1.06 (0.03)
CaO	0.01 (0.02)	0.01 (0.01)	–	–	0.01 (0.01)
Na_2O	0.44 (0.02)	0.49 (0.02)	0.52(0.03)	0.55 (0.12)	0.51 (0.02)
K_2O	8.77 (0.13)	8.64 (0.13)	9.22(0.08)	8.78 (0.06)	8.72 (0.02)
F	0.41 (0.08)	0.48 (0.23)	0.59(0.07)	0.55 (0.12)	0.60 (0.04)
Cl	0.03 (0.02)	0.02 (0.01)	0.03(0.01)	0.04 (0.01)	0.03 (0.01)
EMP Total	94.38 (0.31)	94.82 (0.62)	97.36(0.19)	95.44 (0.33)	93.37 (0.06)
*FeO	4.51	4.59	4.86	5.25	4.65
*Fe_2O_3	6.37	6.50	6.88	7.43	5.83
^+H_2O	2.41 (0.06)	2.41 (0.06)	2.41 (0.06)	2.41 (0.06)	2.41 (0.06)
Total	97.43	97.88	100.46	98.59	96.36

* from Mössbauer analysis. $^+$ from C-H-N elemental analysis.

The Mössbauer spectrum was recorded on about 150 mg of small single crystals dispersed in a cylindrical sample holder. More details about experimental condition and data analysis are described in Scordari *et al*. (1999) and Schingaro *et al*. (2005).

Single-crystal polarized-light FTIR microspectroscopy

Single-crystal micro-FTIR spectra were collected using a NicPlan microscope, equipped with a MCT-A nitrogen-cooled detector and a KBr beamsplitter. Nominal resolution was 4 cm^{-1} and final spectra are the average of 128 scans. Polarized spectra were acquired using a gold wire-grid IR polarizer on a ZnSe substrate, with a spot size ~100 μm. Single (001) cleavage flakes, 100 to 150 μm thick, were oriented under the petrographical microscope using the interference figure as a guide. Optical observations showed the studied Ti-rich mica to be optically negative, with α // [001], thus polarized spectra with **E** // β and **E** // γ were collected on the (001) cleavage plane. The flakes were then mounted on a glass capillary and rotated at 90° under the IR beam using a spindle stage, in order to collect the α-polarization spectra.

Results and discussion

Chemical composition

As a general rule, Mt. Vulture micas are characterized by significant intercrystalline chemical variations particularly regarding the Mg/Fe, Ti and F contents, also in samples from the same stratigraphic layer (Schingaro *et al*., 2001, 2005; Mesto *et al*., 2006). On the contrary, the mica samples examined here turned out to be relatively homogeneous: the minimum-maximum ranges are: SiO_2 35.43–37.22 wt%, Al_2O_3 15.53–16.42 wt%, FeO 9.90–11.94 wt%, MgO 16.92–17.82 wt%, TiO_2 3.12–3.64 wt%, K_2O 8.64–9.22 wt%, fluorine 0.42–0.59 wt% (Table 1).

Calculation of the structural formula for micas is complex owing to the frequent presence of elements with variable valence state and the possible occurrence of vacancies in the structure (Mesto *et al*., 2006). The formulae given in Table 2 were calculated averaging at least 9 microprobe point analyses on the same specimens previously used for the structure refinement; titanium was assumed as Ti^{4+}, the H_2O content was directly determined by C-H-N and the FeO/Fe_2O_3 ratio was obtained from Mössbauer (see below). Possible contaminations by N, C and S were also checked; no N was detected (thus allowing H to be converted into H_2O only), with minor C (~0.09%) and S (< 0.01%). The studied mica samples can be classified as Ti-bearing phlogopite; the alkali site is virtually full, with K dominant and minor Na and Ba (kinoshitalite component). The F content is constant around 0.15 apfu; the most notable feature of the studied samples is the significant deprotonation ($^{O(4)}O^{2-}$ around 0.65 apfu, Table 2).

Table 2. Atomic proportions (a.p.f.u.) as determined by combining EPMA, Mössbauer and C-H-N elemental analysis for the samples given in Table 1. Site coordination numbers according to Rieder *et al.* (1998).

	SA1-3	SA1-5	SA1-9	SA1-51	SA1-52
Si	2.73	2.70	2.75	2.70	2.73
^{IV}Al	1.27	1.30	1.25	1.30	1.27
	4.00	4.00	4.00	4.00	4.00
^{VI}Al	0.17	0.15	0.17	0.09	0.19
Mg	1.98	1.99	1.96	1.92	2.00
Fe^{+2}	0.29	0.29	0.30	0.33	0.30
Fe^{+3}	0.37	0.37	0.38	0.43	0.34
Ti	0.19	0.19	0.18	0.21	0.18
Mn	0.01	0.01	0.01	0.01	0.01
	3.01	3.00	3.00	2.99	3.02
K	0.85	0.84	0.87	0.85	0.85
Na	0.07	0.07	0.08	0.08	0.08
Ba	0.05	0.06	0.03	0.05	0.03
	0.97	0.97	0.98	0.98	0.96
OH	1.23	1.23	1.19	1.22	1.23
F	0.10	0.12	0.14	0.13	0.15
Cl	–	–	–	0.01	0.01

Mössbauer spectroscopy

The prominent features of RT Mössbauer spectrum of SA1 sample are two main asymmetric absorptions centred at about –0.2 and 2.3 mm/s and an evident peak at about 1.0 mm/s (Fig. 1). The former two bands are due to octahedral Fe^{2+}, while the latter represents the high-energy line of two doublets from octahedral Fe^{3+}, the low-energy line being hidden inside the Fe^{2+} absorption. There was no clear evidence for tetrahedral Fe^{3+} in the sample. Spectra were fitted either with pure Lorentzian line-shapes or using a quadrupole splitting distribution (QSD) according to Voigt-based methods (Rancourt & Ping, 1991; Rancourt, 1994a, b; Rancourt *et al*., 1994). In both cases the fitting was obtained with the software "Recoil" (Lagarec & Rancourt, 1998).

The former procedure considered two or three asymmetric doublets due to Fe^{2+} and two symmetric due to Fe^{3+}: this last constraint was introduced because of the strong overlap of the low-velocity components of all the four doublets. The latter method uses a certain number *m* of generalized sites each having its own continuous QSD.

Lorentzian fittings were not considered very satisfactory, therefore only QSD results are reported (see Table 8 and Fig. 1). QSD fittings were performed using two generalized sites, one for Fe^{2+} and the other for Fe^{3+}. The Fe^{2+} QSD was assumed to have three components. The QSD method provided statistically consistent fits and yielded the following results: Fe^{2+} = 44%, Fe^{3+} = 56 %.

X-ray crystal structure refinement

Analysis of the 0*kl* and 1*kl* precession images, done using the APEX software package, showed that all analysed crys-

tals belong to 1*M* polytypes. Anisotropic structure refinements based both on F_o and F_o^2 were carried out in space group *C*2/*m* using a recent version of the program CRYSTALS (Betteridge *et al*., 2003) starting from the data of Hazen & Burnham (1973). It was found that the refined occupancies were almost the same either using F_o or F_o^2 (the results of refinements, in terms of mean atomic numbers (m.a.n.) are shown in Table 7). Fully ionized X-ray scattering factors were used for non-tetrahedral sites, whereas ionized *vs*. neutral species were used for Si and O (Hawthorne *et al*., 1995). Refined parameters were: scale factors, atomic positions, cation occupancy and atomic displacement factors. The final R-values, excluding the H atoms, were in the range 2.55–3.18 %. The samples turned out to be perfectly ordered. Difference-Fourier maps calculated at the end of the refinement with anisotropic displacement factors did not show any significant residual electron density, except for the peak located at the expected position for the hydrogen atoms, at a distance of about 0.69 Å to 0.87 Å from the O(4) oxygen. The H position was then included in the last refinement cycles and lowering of the R-values (2.49–3.10) was obtained. Crystal data, data-collection parameters and some details concerning the structure refinement of the samples investigated here are reported in Table 3.

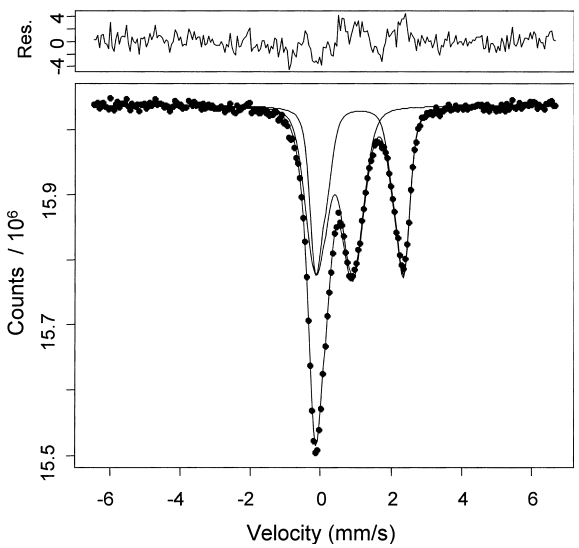

Fig. 1. Room-temperature QSD fitted Mössbauer spectrum for sample SA1.

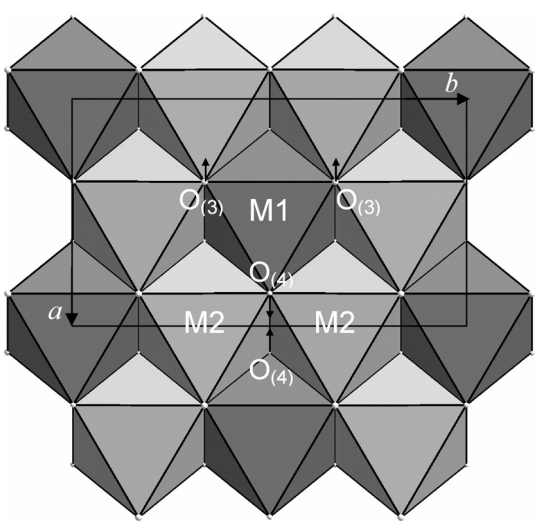

Fig. 2. Undistorted octahedral sheet. The arrows give schematically the distortion mechanisms along [100] related to Ti content: for increasing Ti, the O(3) oxygen moves along [100] toward M2, whereas O(4) moves along [100] away from M1. Unit cell is outlined.

Final atomic coordinates, occupancies and anisotropic and isotropic displacement parameters are given in Table 4. Selected interatomic bond distances in Å are listed in Table 5 whereas the distortion parameters commonly used in crystal chemical studies on micas are reported in Table 6. Finally mean atomic numbers as obtained from structure refinement are compared to those calculated from chemical analyses in Table 7.

Individual tetrahedra are relatively regular, with three distances (T-O(1), T-O(1') and T-O(2)) similar and one slightly longer (T-O(3), see Table 5). Observed mean <T-O> bond distances are consistent (within 1σ) with those calculated from Shannon's (1976) radii (Table 7). Two oxygen radii were considered according to coordination: 1) 1.36 Å for O1 and O2; 2) 1.38 Å for O3. These distances are also close to those calculated using the regression formula of Brigatti & Guggenheim (2002), thus supporting the absence of Fe^{3+} in the tetrahedral site, as indicated by Mössbauer. The differences between the octahedral mean bond distances (<M1-O>, <M2-O>, Tables 5) point to a meso-octahedral character, whereas the difference of the mean electron counts at M1 and M2 are less than 0.5 e^- in agreement with homo-octahedral micas.

Inspection of Table 6 shows an apparent off-centring of the M2 cation towards O(4); as a consequence the mean <M2-O(4)> distance is remarkably short (2.032(1) Å, see Table 5), as already observed for the oxy-biotite from El Joyazo, Spain (Cesare *et al.*, 2003). This result is compatible with a preferential ordering of Ti^{4+} at M2. Additional structural features suggesting a Ti-oxy substitution mechanism in the studied samples are: 1) low values for the *c* lattice parameters (Cesare *et al.*, 2003; Schingaro *et al*., 2005) and 2) a significant shortening of the O(4)-O(4) edge (2.695–2.704 Å) as a consequence of the lengthening of the M1-O4 distance (Schingaro *et al*., 2005), thus reducing the increased electrostatic repulsion due to the presence of high-charge cations (Ti) at neighbouring M2 sites. The displacement of $^{[M2]}$Ti towards O(4) is consistent with the observed hydrogen deficiency (Table 2) and is due to local charge-balance requirements. In addition, for increasing Ti contents, there is a shift of O(3) and O(4) along [100] in opposite directions (Fig. 2, see also Schingaro *et al*., 2005).

The main tetrahedral distortion parameters considered here are: the in-plane rotation angle α, the thickening angle τ and the Δz basal corrugation. The rotation angle is known to be a function of tetrahedral and octahedral sheet compositions and is the most effective mechanism to obtain congruence between tetrahedral and octahedral lateral sizes. The values of α (observed) are in good agreement with the calculated ones (Table 6, in round parentheses) according to the geometrical model proposed by Brigatti & Guggenheim (2002). According to this model $\alpha = \arccos[(3/4)^{1/2}k]$, where

Table 3. Crystal, experimental and refinement data for 1*M* phlogopite samples. In square brackets are quoted the parameters when H is included.

	SA1-3	SA1-5	SA1-9	SA1-51	SA1-52
Space group	*C*2/*m*	*C*2/*m*	*C*2/*m*	*C*2/*m*	*C*2/*m*
a (Å)	5.337(2)	5.334(2)	5.337(2)	5.336(1)	5.335(4)
b (Å)	9.239(3)	9.240(4)	9.238(3)	9.236(2)	9.242(8)
c (Å)	10.237(3)	10.235(4)	10.228(3)	10.223(2)	10.231(8)
β (°)	100.030(2)	100.021(2)	100.050(2)	100.058(1)	100.001(5)
μ (mm^{-1})	4.920	4.940	4.997	5.003	4.967
Tmin/Tmax	0.805	0.725	0.803	0.677	0.703
Cell volume ($Å^3$)	497.1(3)	496.7(4)	496.6(3)	496.1(2)	496.8(7)
Z	2	2	2	2	2
Crystal size	0.18*0.25*0.02 mm^3	0.19*0.28*0.01 mm^3	0.17*0.20*0.02 mm^3	0.25*0.31*0.06 mm^3	0.45*0.27*0.02 mm^3
Radiation type	Mo*Ka* (0.71073Å)	Mo*Ka* (0.71073Å)	Mo*Ka* (0.71073Å)	Mo*Ka* (0.71073Å)	Mo*Ka* (0.71073Å)
Crystal-detector dist. (mm)	40	40	40	40	40
Rotation axis, width (°)	ϕ, ω, 0.5	ϕ, ω, 0.5	ϕ, ω, 0.5	ϕ, ω, 0.5	ϕ, ω, 0.3
Total no. of frames	3198	4853	1465	3787	4271
collec. time per degree (s)	10	10	45	10	10
Redundancy/completeness (%)	4.17/96.0	3.05/98.2	3.64/96.1	2.95/93.0	2.54/92.7
θ range for data collection	2-40°12' (in θ)	2-45°40' (in θ)	2-42° 41'(in θ)	2-46°23' (in θ)	2-45°01' (in θ)
Index range	-9≤h≤4	-9≤h≤10	-8≤h≤10	-10≤h≤10	-9≤h≤10
	-16≤k≤16	-17≤k≤18	-17≤k≤12	-16≤k≤18	-18≤k≤10
	-18≤l≤18	-19≤l≤20	-19≤l≤19	-20≤l≤19	-19≤l≤19
Reflections measured/rejected/ unique	25369/1/1611 [Rint = 0.0401]	21893/36/1927 [Rint = 0.0376]	13307/200/1823 [Rint = 0.0239]	23290/122/2132 [Rint = 0.0367]	16980/16/1931 [Rint = 0.0340]
Reflections used	785 with I>3σ(I)	1005 with I>3σ(I)	1219 with I>3σ(I)	1703 with I>3σ(I)	874 with I>3σ(I)
No. of refined parameters	68 [71]	68 [71]	68 [71]	68 [71]	68 [71]
d_{min} (Å)	0.551	0.497	0.524	0.491	0.502
Goof[a]	0.676 [0.676]	0.767 [0.758]	1.002 [0.994]	1.022 [0.991]	0.922 [0.920]
R_1[b] (on *F*)	0.0287 [0.282]	0.0281 [0.0274]	0.0318 [0.0310]	0.0255 [0.0249]	0.0281 [0.0273]
wR_2[c] (on F^2)	0.0804 [0.0799]	0.0764 [0.0753]	0.0819 [0.0789]	0.0685 [0.0678]	0.0685 [0.0664]
$(\Delta/\sigma)_{max}$	0.0210	0.0242	0.0206	0.0222	0.0174
$\Delta\rho_{min}$, $\Delta\rho_{max}$ ($e/Å^3$)	-0.367, 0.671	-0.318, 0.751	-0.634, 0.841	-0.684, 0.681	-0.556, 0.702

[a] Goodness-of-fit = $[\Sigma[w(F_o^2-F_c^2)^2]/(N-P)]^{1/2}$, where *N* and *P* are the number of reflections and parameters, respectively.

[b] $R_1 = \Sigma[|F_o| - |F_c|]/\Sigma|F_o|$

[c] $wR_2 = [\Sigma[w(F_o^2-F_c^2)^2]/\Sigma[w(F_o^2)^2]]^{1/2}$, where $w = 1/[\sigma^2(F_o^2) + (xP)^2 + yP]$; $P = [0.333*\mathrm{Max}(F_o^2,0) + 0.667*F_c^2]$: SA1-3 [x = 0(0); y = 0(0)]; SA1-5 [x = 0(0); y = 0(0)]; SA1-9 [x = 0.047(0.0442); y = 0.260(0.285)]; SA1-51 [x = 0.037(0.036); y = 0.251(0.146)]; SA1-52 [x = 0.046(0.044); y = 0(0)];

Table 4. Crystallographic coordinates, occupancies, equivalent isotropic (Å^2) and anisotropic displacement parameters.

Sample SA1-3

Atom	*x*	*y*	*z*	Occupancy	$U_{iso/equiv}$	U_{11}	U_{22}	U_{33}	U_{23}	U_{13}	U_{12}
K	0.0000	0.5000	0.0000	1.0657(8)	0.0321	0.0309(5)	0.0332(6)	0.0321(5)	0.0000	0.0052(4)	0.0000
Mg1	0.0000	0.0000	0.5000	0.7460(8)	0.0114	0.0095(4)	0.0094(4)	0.0158(5)	0.0000	0.0032(3)	0.0000
Fe1	0.0000	0.0000	0.5000	0.2539(7)	0.0114	0.0095(4)	0.0094(4)	0.0158(5)	0.0000	0.0032(3)	0.0000
Mg2	0.0000	0.33500(7)	0.5000	0.7496(8)	0.0120	0.0081(2)	0.0136(3)	0.0143(3)	0.0000	0.0017(2)	0.0000
Fe2	0.0000	0.33500(7)	0.5000	0.2504(7)	0.0120	0.0081(2)	0.0136(3)	0.0143(3)	0.0000	0.0017(2)	0.0000
Si	0.07516(9)	0.16682(5)	0.22580(6)	1	0.0117	0.0102(2)	0.0108(2)	0.0142(2)	0.0000(2)	0.00212(16)	0.00004(17)
O1	0.3306(3)	0.22528(19)	0.16875(15)	1	0.0213	0.0183(6)	0.0261(8)	0.0201(7)	-0.0042(6)	0.0051(5)	-0.0059(6)
O2	0.0068(4)	0.0000	0.1696(2)	1	0.0204	0.0262(10)	0.0162(9)	0.0174(9)	0.0000	-0.0003(8)	0.0000
O3	0.1307(3)	0.16761(14)	0.39126(15)	1	0.0128	0.0126(5)	0.0123(5)	0.0139(5)	-0.0001(5)	0.0031(4)	0.0000(4)
O4	0.1324(4)	0.5000	0.3989(2)	1	0.0142	0.0141(8)	0.0150(8)	0.0129(9)	0.0000	0.0007(7)	0.0000
H	0.119(12)	0.5000	0.313(6)	0.7105(10)	0.0142	0.0141(8)	0.0150(8)	0.0129(9)	0.0000	0.0007(7)	0.0000

Sample SA1-5

Atom	*x*	*y*	*z*	Occupancy	$U_{iso/equiv}$	U_{11}	U_{22}	U_{33}	U_{23}	U_{13}	U_{12}
K	0.0000	0.5000	0.0000	1.0653(7)	0.0308	0.0304(3)	0.0304(4)	0.0316(4)	0.0000	0.0055(3)	0.0000
Mg1	0.0000	0.0000	0.5000	0.7554(8)	0.0109	0.0098(3)	0.0080(3)	0.0158(3)	0.0000	0.0042(2)	0.0000
Fe1	0.0000	0.0000	0.5000	0.2447(6)	0.0109	0.0098(3)	0.0080(3)	0.0158(3)	0.0000	0.0042(2)	0.0000
Mg2	0.0000	0.33555(6)	0.5000	0.7462(8)	0.0119	0.00852(16)	0.0131(2)	0.0142(2)	0.0000	0.00214(15)	0.0000
Fe2	0.0000	0.33555(6)	0.5000	0.2538(7)	0.0119	0.00852(16)	0.0131(2)	0.0142(2)	0.0000	0.00214(15)	0.0000
Si	0.07514(7)	0.16687(4)	0.22577(4)	1	0.0107	0.00994(14)	0.00927(17)	0.01315(17)	0.00008(15)	0.00240(12)	0.00008(13)
O1	0.3303(2)	0.22552(15)	0.16832(12)	1	0.0205	0.0185(4)	0.0248(6)	0.0189(5)	-0.0037(5)	0.0051(4)	-0.0064(4)
O2	0.0063(3)	0.0000	0.16935(18)	1	0.0201	0.0264(7)	0.0140(7)	0.0185(7)	0.0000	0.0001(6)	0.0000
O3	0.13101(19)	0.16747(12)	0.39139(12)	1	0.0127	0.0123(3)	0.0118(4)	0.0141(4)	0.0006(4)	0.0028(3)	0.0001(3)
O4	0.1324(3)	0.5000	0.39917(16)	1	0.0134	0.0129(5)	0.0147(6)	0.0124(6)	0.0000	0.0016(5)	0.0000
H	0.115(9)	0.5000	0.332(5)	0.7027(10	0.0134	0.0129(5)	0.0147(6)	0.0124(6)	0.0000	0.0016(5)	0.0000

Sample SA1-9

Atom	*x*	*y*	*z*	Occupancy	$U_{iso/equiv}$	U_{11}	U_{22}	U_{33}	U_{23}	U_{13}	U_{12}
K	0.0000	0.5000	0.0000	1.0170(7)	0.0309	0.0320(4)	0.0305(4)	0.0302(4)	0.0000	0.0054(3)	0.0000
Mg1	0.0000	0.0000	0.5000	0.7403(8)	0.0095	0.0091(3)	0.0069(2)	0.0128(3)	0.0000	0.0035(2)	0.0000
Fe1	0.0000	0.0000	0.5000	0.2589(6)	0.0095	0.0091(3)	0.0069(2)	0.0128(3)	0.0000	0.0035(2)	0.0000
Mg2	0.0000	0.33610(5)	0.5000	0.7256(8)	0.0107	0.00755(17)	0.01274(19)	0.0117(2)	0.0000	0.00109(14)	0.0000
Fe2	0.0000	0.33610(5)	0.5000	0.2742(7)	0.0107	0.00755(17)	0.01274(19)	0.0117(2)	0.0000	0.00109(14)	0.0000
Si	0.07503(7)	0.16690(4)	0.22570(4)	1	0.0091	0.00903(14)	0.00808(14)	0.01012(15)	0.00019(12)	0.00158(10)	0.00009(11)
O1	0.3299(2)	0.22619(14)	0.16852(11)	1	0.0184	0.0178(4)	0.0232(5)	0.0150(4)	-0.0033(4)	0.0049(4)	-0.0063(4)
O2	0.0087(3)	0.0000	0.16952(16)	1	0.0185	0.0261(7)	0.0133(6)	0.0146(6)	0.0000	-0.0004(5)	0.0000
O3	0.13035(18)	0.16764(10)	0.39156(10)	1	0.0110	0.0109(3)	0.0109(3)	0.0113(3)	0.0003(3)	0.0022(3)	0.0004(3)
O4	0.1324(3)	0.5000	0.39905(14)	1	0.0119	0.0122(5)	0.0133(5)	0.0100(5)	0.0000	0.0012(4)	0.0000
H	0.114(9)	0.5000	0.317(4)	0.6806(10)	0.0119	0.0122(5)	0.0133(5)	0.0100(5)	0.0000	0.0012(4)	0.0000

Sample SA1-51

Atom	*x*	*y*	*z*	Occupancy	$U_{iso/equiv}$	U_{11}	U_{22}	U_{33}	U_{23}	U_{13}	U_{12}
K	0.0000	0.5000	0.0000	1.0451(5)	0.0301	0.0305(2)	0.0306(2)	0.0292(2)	0.0000	0.00536(17)	0.0000
Mg1	0.0000	0.0000	0.5000	0.7249(6)	0.0098	0.00893(14)	0.00821(13)	0.01293(15)	0.0000	0.00364(10)	0.0000
Fe1	0.0000	0.0000	0.5000	0.2736(4)	0.0098	0.00893(14)	0.00821(13)	0.01293(15)	0.0000	0.00364(10)	0.0000
Mg2	0.0000	0.33579(3)	0.5000	0.7235(6)	0.0108	0.00721(10)	0.01362(11)	0.01140(10)	0.0000	0.00130(7)	0.0000
Fe2	0.0000	0.33579(3)	0.5000	0.2760(5)	0.0108	0.00721(10)	0.01362(11)	0.01140(10)	0.0000	0.00130(7)	0.0000
Si	0.07504(4)	0.16693(2)	0.22557(2)	1	0.0090	0.00835(8)	0.00903(8)	0.00963(8)	0.00014(5)	0.00167(6)	0.00000(5)
O1	0.32969(14)	0.22605(8)	0.16825(7)	1	0.0190	0.0175(2)	0.0249(3)	0.0153(2)	-0.0035(2)	0.00448(19)	-0.0067(2)
O2	0.0083(2)	0.0000	0.16922(9)	1	0.0190	0.0266(4)	0.0138(3)	0.0149(3)	0.0000	-0.0007(3)	0.0000
O3	0.13067(11)	0.16769(5)	0.39140(6)	1	0.0111	0.01136(19)	0.01192(18)	0.01001(17)	0.00010(13)	0.00159(14)	0.00027(13)
O4	0.13192(16)	0.5000	0.39899(8)	1	0.0126	0.0122(3)	0.0147(3)	0.0107(3)	0.0000	0.0018(2)	0.0000
H	0.112(6)	0.5000	0.331(3)	0.6949(7)	0.0126	0.0122(3)	0.0147(3)	0.0107(3)	0.0000	0.0018(2)	0.0000

Sample SA1-52

atom	*x*	*y*	*z*	Occupancy	$U_{iso/equiv}$	U_{11}	U_{22}	U_{33}	U_{23}	U_{13}	U_{12}
K	0.0000	0.5000	0.0000	1.0091(7)	0.0315	0.0313(5)	0.0321(5)	0.0316(6)	0.0000	0.0068(4)	0.0000
Mg1	0.0000	0.0000	0.5000	0.7370(8)	0.0107	0.0096(4)	0.0084(3)	0.0148(5)	0.0000	0.0042(3)	0.0000
Fe1	0.0000	0.0000	0.5000	0.2625(6)	0.0107	0.0096(4)	0.0084(3)	0.0148(5)	0.0000	0.0042(3)	0.0000
Mg2	0.0000	0.33530(7)	0.5000	0.7303(8)	0.0116	0.0081(2)	0.0132(2)	0.0137(3)	0.0000	0.0022(2)	0.0000
Fe2	0.0000	0.33530(7)	0.5000	0.2696(7)	0.0116	0.0081(2)	0.0132(2)	0.0137(3)	0.0000	0.0022(2)	0.0000
Si	0.07514(9)	0.16686(5)	0.22597(5)	1	0.0103	0.00939(18)	0.00923(16)	0.0125(2)	0.0000(2)	0.00268(16)	-0.0001(2)
O1	0.3301(3)	0.22632(16)	0.16888(14)	1	0.0201	0.0182(6)	0.0246(7)	0.0181(6)	-0.0034(6)	0.0054(5)	-0.0053(6)
O2	0.0084(4)	0.0000	0.1697(2)	1	0.0197	0.0257(10)	0.0152(7)	0.0172(9)	0.0000	0.0004(8)	0.0000
O3	0.1306(2)	0.16728(13)	0.39175(13)	1	0.0121	0.0122(5)	0.0114(4)	0.0129(5)	-0.0006(5)	0.0024(4)	-0.0001(5)
O4	0.1317(4)	0.5000	0.39840(19)	1	0.0125	0.0118(8)	0.0133(7)	0.0125(8)	0.0000	0.0025(7)	0.0000
H	0.113(9)	0.5000	0.317(5)	0.7015(10)	0.0125	0.0118(8)	0.0133(7)	0.0125(8)	0.0000	0.0025(7)	0.0000

Table 5. Results of structure refinement in space group *C*2/*m*: selected bond distances.

	SA1-3	SA1-5	SA1-9	SA1-51	SA1-52
T-O(1)	1.664(2)	1.664(1)	1.665(1)	1.6631(7)	1.664(2)
T-O(1')	1.665(2)	1.665(1)	1.662(1)	1.6633(7)	1.661(1)
T-O(2)	1.663(1)	1.665(1)	1.6618(7)	1.6625(4)	1.6630(9)
T-O(3)	1.668(2)	1.669(1)	1.670(1)	1.6693(6)	1.670(1)
<T-O>	1.665	1.666	1.665	1.6646	1.665
M1-O(4)(x2)	2.052(2)	2.051(2)	2.051(1)	2.0532(8)	2.057(2)
M1-O(3)(x4)	2.096(1)	2.095(1)	2.093(1)	2.0948(5)	2.091(1)
<M1-O>	2.081	2.080	2.079	2.0809	2.080
M2-O(4)(x2)	2.037(2)	2.031(1)	2.028(1)	2.0288(6)	2.036(1)
M2-O(3)(x2)	2.088(1)	2.085(1)	2.088(1)	2.0865(6)	2.086(1)
M2-O(3')(x2)	2.095(2)	2.099(1)	2.099(1)	2.0975(6)	2.096(1)
<M2-O>	2.073	2.072	2.072	2.0709	2.073
<M-O>	2.076	2.075	2.074	2.0742	2.075
K-O(1)(x4)	2.946(2)	2.944(2)	2.951(1)	2.9477(7)	2.954(1)
K-O(1')(x4)	3.388(2)	3.383(1)	3.378(1)	3.3761(8)	3.380(2)
K-O(2)(x2)	2.949(2)	2.945(1)	2.955(2)	2.951(1)	2.955(2)
K-O(2')(x2)	3.396(2)	3.395(2)	3.386(2)	3.386(1)	3.387(2)
$<K\text{-}O>_{inner}$	2.947	2.944	2.952	2.949	2.954
$<K\text{-}O>_{outer}$	3.391	3.387	3.381	3.379	3.382
<K-O>	3.169	3.166	3.167	3.164	3.168

Table 6. Selected parameters derived from the structure refinements in space group *C*2/*m*.

	SA1-3	SA1-5	SA1-9	SA1-51	SA1-52
t_{tet} [Å]	2.240	2.245	2.244	2.243	2.243
BLD_T	0.103	0.093	0.181	0.135	0.174
$Volume_T$ [Å^3]	2.37	2.37	2.37	2.37	2.37
TQE	1.0001	1.0002	1.0002	1.0002	1.0002
TAV	0.701	0.933	0.771	0.831	0.765
τ [°]	110.102	110.235	110.147	110.183	110.144
α [°]	9.71(9.19)	9.63(9.21)	9.36(9.06)	9.40(8.91)	9.33(9.04)
Δz [Å]	0.0081	0.0111	0.0101	0.0091	0.0081
D.M. [Å]	0.568	0.571	0.567	0.565	0.564
$\Psi_{M(1)}$ [°]	59.06	59.10	59.14	59.13	59.09
$\Psi_{M(2)}$ [°]	58.92	58.96	59.01	58.96	58.98
$BLD_{M(1)}$	0.927	0.950	0.891	0.889	0.709
$ELD_{M(1)}$	5.190	5.237	5.280	5.277	5.229
$BLD_{M(2)}$	1.165	1.319	1.409	1.360	1.175
$ELD_{M(2)}$	5.027	5.071	5.132	5.078	5.095
$Shift_{M(2)}$ [Å]	0.015	0.021	0.026	0.023	0.018
Volume $_{M(1)}$ [Å]	11.81	11.79	11.76	11.80	11.77
$OQE_{M(1)}$	1.0120	1.0123	1.0124	1.0124	1.0121
$OAV_{M(1)}$	38.826	39.576	40.113	40.116	39.311
Volume $_{M(2)}$ [Å^3]	11.68	11.66	11.65	11.64	11.67
$OQE_{M(2)}$	1.0113	1.0116	1.0119	1.0116	1.0116
$OAV_{M(2)}$	36.815	37.508	38.464	37.640	37.685
$E_uM(1)/e_sM(1)$	1.1095	1.1105	1.1115	1.1114	1.1104
$E_uM(2)/e_sM(2)$	1.1059	1.1068	1.1082	1.1070	1.1074
t_{oct} [Å]	2.140	2.137	2.133	2.135	2.136
t_{int} [Å]	3.409	3.400	3.401	3.394	3.409
$\Delta_{K\text{-}O4}$ [Å]	0.444	0.443	0.428	0.430	0.428
$t_{K\text{-}O4}$ [Å]	3.960	3.962	3.957	3.954	3.953

Note: t_{tet}: tetrahedral sheet thickness calculated from z coordinates of basal and apical O atoms; TQE: tetrahedral quadratic elongation (Robinson *et al*. 1971); TAV: tetrahedral angle variance (Robinson *et al*. 1971); τ: tetrahedral flattening angle; α: tetrahedral rotation angle (Hazen & Burnham, 1973); in parentheses values calculated according Brigatti & Guggenheim, 2002; Δz: departure from complanarity of the basal O atoms, (Guven, 1971); D.M.: dimensional misfit between tetrahedral and octahedral sheets (Toraya, 1981); ψ: octahedral flattening angles (Donnay *et al*., 1964a, b); BLD: bond-length distortions (Renner & Lehmann 1986); ELD: edge-length distortion (Renner & Lehman, 1986); $Shift_{M2}$: off-center shift of the M2 cation defined as the distance between the refined position of cation and the geometrical center of M2 site (coordinates: x/a = 0.0, y/b = 0.8333, z/c = 0.5); OQE: octahedral quadratic elongation (Robinson *et al.,* 1971); OAV: octahedral angle variance (Robinson *et al*., 1971); e_u,e_s: mean lengths of unshared and shared edges (Toraya, 1981), respectively; t_{oct}: octahedral sheet thickness (Toraya, 1981); t_{int} calculated from the z coordinates of basal O atoms; $\Delta_{K\text{-}O4} = <K\text{-}O>_{outer}\text{-}<K\text{-}O>_{inner}$; $t_{K\text{-}O4}$: projection of K-O4 distance along c*.

Table 7. Mean atomic numbers of cation sites and octahedral and tetrahedral mean distances, as determined by structure refinement using both Fo and Fo^2 (in square brackets) and chemical analyses (EMPA). See text for details.

	SA1-3	SA1-5	SA1-9	SA1-51	SA1-52
$e^-_{(M1+M2)X\text{-}ref}$	46.57[46.50]	46.53[46.56]	47.29[47.25]	47.53[47.50]	47.22[47.05]
$e^-_{(M1+M2)\ EMPA}$	47.33	47.48	47.68	48.87	47.01
$e^-_{(M1)\ X\text{-}ref}$	15.55[15.53]	15.43[15.46]	15.62[15.60]	15.81[15.79]	15.67[15.63]
$e^-_{(M1)\ EMPA}$	15.63	15.66	15.68	16.21	15.55
$e^-_{(M2)\ X\text{-}ref}$	15.51[15.48]	15.55[15.55]	15.84[15.83]	15.86[15.85]	15.77[15.71]
$e^-_{(M2)\ EMPA}$	15.85	15.91	16.00	16.33	15.73
K $e^-_{X\text{-}ref}$	20.25[20.19]	20.24[20.21]	19.32[19.37]	19.86[19.82]	19.17[19.22]
K e^-_{EMPA}	20.00	20.30	18.97	19.95	18.79
T $e^-_{X\text{-}ref}$	13.78[13.76]	13.69[13.68]	13.73[13.74]	13.61[13.58]	13.84[13.77]
T e^-_{EMPA}	13.68	13.67	13.69	13.68	13.68
Σ^+	22.66	22.63	22.65	22.65	22.59
Σ^-	22.65	22.62	22.64	22.64	22.58
$\langle T\text{-}O\rangle_{X\text{-}ref}$	1.665(2)	1.666(1)	1.665(1)	1.6646(6)	1.665(1)
$\langle T\text{-}O\rangle_{EMPA}$	1.666	1.667	1.666	1.666	1.667
$\langle M\text{-}O\rangle_{X\text{-}ref}$	2.076(2)	2.075(1)	2.074(1)	2.0742(6)	2.075(1)
$\langle M\text{-}O\rangle_{EMPA}$	2.067	2.069	2.068	2.071	2.068

Table 8. Mössbauer parameters obtained by QSD method.

	χ^2	Specie	$\delta_0{}^\dagger$ (mm/s)	A_-/A_+	ΔE_Q (mm/s)	σ	P (%)	A (%)
		Fe^{2+}	1.1122	1*	1.95	0.289	35	43.93(39)
SA1	2.19							
			1.1122	1*	2.516	0.228	65	
		Fe^{3+}	0.3925	1*	1.023	0.523	100*	56.07(39)

$^\dagger\delta = 0$ during fitting, *fixed parameter

k is the ratio between the $\langle O\text{-}O\rangle_u$ unshared octahedral edges and $\langle O\text{-}O\rangle_b$ tetrahedral basal edges. Note that α decreases as $\langle O\text{-}O\rangle_u$ increases. As discussed above, the increasing Ti content causes the opposite movement of oxygens O(3) and O(4) along [100] inducing longer <O-O> unshared bond distances. Therefore the decrease of α rotation angle is correlated to the increase of Ti content, indicating the important role of the Ti substitution mechanism for the fit between octahedral and tetrahedral sheets.

The angle τ of the tetrahedra is a measure of the distortion of the tetrahedra by elongation or compression normal to the sheet. This angle changes with Si content, tetrahedral cation position and mean value of basal oxygen distance bonds. Therefore τ is another important distortion parameter that evaluate the dimensional adjustments between tetrahedral and octahedral sheets. Measured τ angles greater than the ideal tetrahedral angle of 109.47° indicate tetrahedra elongated along T-O apical direction. For SA1 samples the elongation is negligible (Table 6).

The small effect of the basal oxygen atom plane corrugation has positive values in our samples reflecting the slight enlargement of the M1 with respect to the M2 sites.

The interlayer site show differences (ΔK-O) between the inner and outer K-O bonds consistent with the rotation angle α (Tyrna & Guggenheim, 1991; Guggenheim & Frimmel, 1999). The shortening of the K-O(4) distance (Table 5) and of *c* edge (Table 3) are an other indication of Ti-oxy substitution (Cruciani & Zanazzi, 1994; Cesare *et al*., 2003; Schingaro *et al*., 2005) as a consequence of the decreased interaction between the proton and the interlayer cation.

Single-crystal FTIR spectroscopy

Polarized-light spectra and the orientation of the O-H dipoles

Pleochroic measurements on oriented crystal sections provide the orientation of the absorber within the structure (*e.g.* Libowitzky & Rossman, 1996); for micas, there are few IR

Table 9. Structural formulae and cation partitioning.

SA1-3	$(K_{.855}Na_{.065}Ba_{.054}\ Ca_{.001}[]_{.025})(Al_{.171}Mg_{1.978}Mn_{.009}Fe^{2+}_{.287}Fe^{3+}_{.365}Ti_{.186}\ Cr_{.004})(Si_{\ 2.727}\ Al_{\ 1.273})\ O_{\ 10.654}\ F_{.101}\ Cl_{.004}OH_{\ 1.241}$ M1: $Mg_{0.676}Mn_{.009}Fe^{2+}_{.131}\ Fe^{3+}_{.115}\ Al_{.069}$; M2: $Mg_{0.651}Fe^{2+}_{.078}Fe^{3+}_{.125}Ti_{.093}\ Al_{.051}\ Cr_{.002}$
SA1-5	$(K_{.838}\ Na_{.072}\ Ba_{.063}\ Ca_{.001}\ []_{.026})(Al_{.147}\ Mg_{1.989}\ Mn_{.010}\ Fe^{2+}_{.292}\ Fe^{3+}_{.372}\ Ti_{.187}Cr_{.003})\ (Si_{\ 2.695}\ Al_{\ 1.305})\ O_{\ 10.621}\ F_{.115}\ Cl_{.002}OH_{\ 1.262}$ M1: $Mg_{0.683}Mn_{.010}Fe^{2+}_{.136}Fe^{3+}_{.112}\ Al_{.059}$; M2: $Mg_{0.653}Fe^{2+}_{.078}Fe^{3+}_{.130}Ti_{.0935}\ Al_{.044}\ Cr_{.0015}$
SA1-9	$(K_{.867}Na_{.074}Ba_{.030}[]_{.029})(Al_{.168}Mg_{1.957}Mn_{.011}Fe^{2+}_{.300}Fe^{3+}_{.382}Ti_{.180}\ Cr_{.002})(Si_{\ 2.743}\ Al_{\ 1.257})\ O_{\ 10.644}\ F_{.137}\ Cl_{.004}OH_{\ 1.215}$ M1: $Mg_{0.673}Mn_{.011}Fe^{2+}_{.129}\ Fe^{3+}_{.119}\ Al_{.068}$; M2: $Mg_{0.642}Fe^{2+}_{.086}Fe^{3+}_{.131}Ti_{.090}\ Al_{.050}\ Cr_{.001}$
SA1-51	$(K_{.851}Na_{.081}Ba_{.052}[]_{.016})(Al_{.093}Mg_{1.916}Mn_{.012}\ Fe^{2+}_{.334}Fe^{3+}_{.425}Ti_{.208}\ Cr_{.002}[]_{.010})(Si_{\ 2.702}\ Al_{\ 1.298})\ O_{\ 10.640}\ F_{.132}\ Cl_{.005}OH_{\ 1.223}$ M1: $Mg_{0.644}Mn_{.012}Fe^{2+}_{.154}Fe^{3+}_{.141}\ Al_{.039}\ []_{.010}$; M2: $Mg_{0.636}Fe^{2+}_{.090}Fe^{3+}_{.142}Ti_{.104}\ Al_{.027}\ Cr_{.001}$
SA1-52	$(K_{.851}Na_{.076}Ba_{.032}\ Ca_{.001}\ []_{.040})(Al_{.178}Mg_{1.997}Mn_{.011}Fe^{2+}_{.298}Fe^{3+}_{.336}Ti_{.179}\ Cr_{.001})(Si_{\ 2.722}\ Al_{\ 1.278})\ O_{\ 10.575}\ F_{.133}\ Cl_{.005}OH_{\ 1.287}$ M1: $Mg_{0.681}Mn_{.011}Fe^{2+}_{.138}Fe^{3+}_{.100}\ Al_{.070}$; M2: $Mg_{0.658}Fe^{2+}_{.080}Fe^{3+}_{.118}Ti_{.0895}\ Al_{.054}\ Cr_{.0005}$

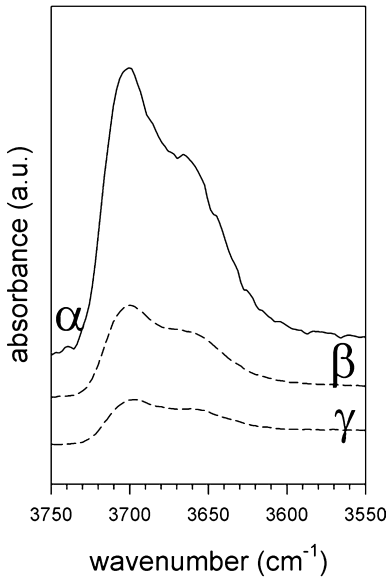

Fig. 3. Polarized-light OH-stretching FTIR spectra of sample SA3 from Cava St. Antonio (Mt. Vulture, Italy). Spectra plotted with the same absorbance scale.

pleochroic works in the literature (*e.g.* Serratosa & Bradley, 1962; Vedder & McDonald, 1963). Figure 3 shows the spectra collected along the three principal optical directions, plotted with the same absorbance scale. Serratosa & Bradley (1962) showed that, for phlogopite, the absorbance is close to zero when the electric field vector (**E**) of the light is normal to the O-H bond axis. In agreement with this observation, the spectra displayed in Fig. 3 suggest that, in Ti-rich phlogopites from Mt. Vulture, the O-H bond axes are strongly polarized along the α direction, *i.e.* // to *c**. The absorbance is greatly reduced along the β and γ directions, which lie on the (001) plane (Fig. 3). The measured dichroic ratio (A_{max}/A_{min}) of a particular absorption (in our case ν(O-H)) relates directly to the orientation of the transition moment for that vibrational mode (*e.g.* Turrell, 1972), according to $A_{max}/A_{min} = \cot^2\theta$ (where A_{max} = maximum integrated absorbance, A_{min} = minimum integrated absorbance and θ = angle between the O-H bond axis and A_{min}, see also Johnston *et al.*, 1990, and Libowitzky & Rossman, 1996). The data extracted from the spectra of Fig. 3 allow us to calculate an angle O-H ^ α ~ 23° and O-H ^ γ ~ 56°.

Spectrum fitting

The IR pattern of the investigated mica (Fig. 3) is clearly composed of several overlapping components, with two maxima at ~ 3700 and 3665 cm^{-1}, respectively. The digitized spectra were fitted by interactive optimization followed by least-squares refinement (Della Ventura *et al.*, 1996); the background was treated as linear and all bands were modelled as symmetric Gaussians (Strens, 1974). The spectra were fitted (Fig. 4) to the smallest number of peaks needed for an accurate description of the spectral profile. The distribution of absorption, y, as a function of energy (wave number, x) was described by the relation $y = A \exp [- 0.5 (x - P / W)^2]$ where A is the amplitude, P is the peak centroid, and W

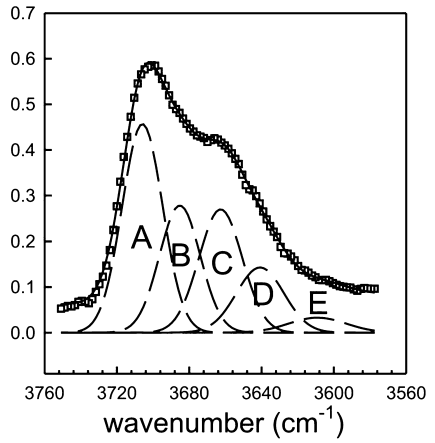

Fig. 4. Fitted OH-stretching α-polarization spectrum of sample SA3; the component bands are indicated.

is the full-width at half-maximum height (FWHM). Peak widths were constrained to values approximately equal to those known for similar mica compositions (Redhammer *et al.*, 2000).

Band assignment

Assignment of the bands of Fig. 4 can be based on the known IR spectroscopy data for these kind of compounds (*e.g.* Redhammer *et al.*, 2000) and considering the chemical composition and the cation partition of the sample. The simplified formula of the studied mica is $K(Mg_{2.0}Fe^{2+}_{0.3}M^{3+}_{0.5}Ti_{0.2})(Si_{2.7}Al_{1.3})O_{10}(OH_{1.3}O^{2-}_{0.6}F_{0.1})$, with $M^{3+} = Fe^{3+}$, Al^{3+} (Table 2). The features to consider for the assignment of the bands present in the spectrum according to local structural configurations are:

(1) the studied mica has a virtually full A-site, with K dominant;
(2) the octahedral divalent cation is predominantly Mg, but there is a significant amount of Fe^{2+}; there is in addition significant M^{3+} which is predominantly Fe^{3+}, and a notable amount of Ti^{4+} (0.2 apfu);
(3) there is ~0.65 O^{2-} apfu at the anionic site; this raises the possibility of OH-OH, OH-O^{2-} and O^{2-}-O^{2-} local arrangements; obviously, O^{2-}-O^{2-} arrangements would be invisible to infrared whereas both OH-OH and OH-O^{2-} arrangements are expected to give a spectroscopic signal in the OH-stretching region (Della Ventura *et al.*, unpubl. data).

The presence of two divalent cations (Mg-Fe^{2+}) at the octahedral M(1,2) sites is expected to generate a defined quartet of bands in the FTIR OH-spectrum (bands N: Vedder, 1964), which can be assigned to the local configurations MgMgMg-OH, MgMgFe^{2+}-OH, Mg$Fe^{2+}Fe^{2+}$-OH, and $Fe^{2+}Fe^{2+}Fe^{2+}$-OH. In our case, due to the predominance of Mg at the octahedral sites, the band related to the MgMgMg-OH configuration is likely to be the most intense. The relative distribution of divalent and trivalent (Fe^{3+}, Al^{3+}) cations produces the appearance in the spectrum of I (= impurity) bands (Vedder, 1964). In our case these

bands are expected to be of type $M^{2+}M^{2+}M^{3+}$, with M^{2+} = (Mg^{2+}, Fe^{2+}), and M^{3+} = (Fe^{3+}, Al^{3+}). These bands are displaced to lower frequency with respect the $M^{2+}M^{2+}M^{2+}$ bands by about 40 cm^{-1} for Fe^{3+} (Redhammer *et al*., 2000). The structural details discussed above show that the entry of Ti in the studied samples occurs *via* oxy-substitution; accordingly $^{[6]}Ti$ is strongly ordered at M2 and is locally associated with $^{O(4)}O^{2-}$. Brigatti *et al*. (1991) observed that the increase of Ti content causes an increasing distortion in M1 site, and accordingly located Ti in this position. Later Cruciani & Zanazzi (1994) showed that some structural features of Ti-bearing micas are diagnostic of the occurrence of Ti-oxy substitutions. In particular the off-centre shift of the M2 cation toward O4 indicates the preferential partitioning of Ti into M2. This structural detail has been recently confirmed by Cesare *et al*. (2003), Brigatti *et al*. (2003) and Schingaro *et al*. (2005). Note that in the oxy-substitution (Ti^{4+} + 2 O^{2-} ⇒ (Mg,Fe^{2+}) + 2 OH^-) *each* Ti is associated with *two* O^{2-}, hence configurations like $M^{2+}M^{2+}Ti^{4+}$ would be invisible to infrared, being associated to O^{2-} – O^{2-} local arrangements. Considering the above points, we can assign the bands in the spectrum of Fig. 4 as follows.

– Band A is assigned to the MgMgMg-OH (N-band) configuration; its position (3706 cm^{-1}) is very close to that measured for end-member phlogopite (*e.g*. Serratosa & Bradley, 1962).
– Band B is shifted by ~20 cm^{-1} to lower frequency with respect to band A. Recent work (Robert *et al*., 1999) shows that in A-site filled amphiboles, there is vibrational coupling of two OH-groups across the A-site cavity through the resident A atom. This feature has a significant influence on the infrared spectrum, because local arrangements involving an OH group are significantly affected by adjacent arrangements involving O^{2-} at the anionic site, and are thus displaced to lower frequency by ~20 cm^{-1} (Della Ventura *et al*., unpublished data). A similar effect can be expected for the closely related micas studied here, thus B band is assigned to the MgMgMg-OH configuration (N-band) whose OH-group are involved in OH-O^{2-} local arrangements.
– Band C is assigned to the MgMgFe^{3+}-OH (I-band) configuration; it is shifted by 40 cm^{-1} toward lower frequency with respect to band B, in agreement with the data of Redhammer *et al*. (2000).
– Band D is assigned to the MgMgFe^{3+}-OH (I-band) configuration whose OH-groups are involved in OH-O^{2-} local arrangements.

Assignment of band E is ambiguous; however, the intensity of this component is very low.

Final refined data and band assignment are given in Table 10. An important observation from Table 10 is that the relative intensity of bands B + D, assigned to configurations involving OH-O^{2-} local arrangements is ~36 % out of the total intensity. Considering the error introduced by neglecting in the fitting, for simplicity, the N-bands due to mixed Mg-Fe^{2+} trimers, this value can be considered in excellent agreement with the analyzed O^{2-}/OH ratio (Table 2), supporting the idea that both the fitting and the band assignment are correct.

Crystal-chemistry of Ti-rich phlogopite from Mt. Vulture

It is known (Cruciani & Zanazzi, 1994; Cesare *et al*., 2003; Waters *et al*., 2002, Dyar *et al*. 1993) that the most common substitution mechanisms involving octahedral Ti^{4+} in micas are:

(1) 2 $^{VI}R^{2+} \leftrightarrow {}^{VI}Ti^{4+} + {}^{VI}\square$, known as Ti-vacancy
(2) $^{VI}R^{2+}$ + 2 $^{IV}Si^{4+} \leftrightarrow {}^{VI}Ti^{4+}$ + 2 $^{IV}Al^{3+}$, known as Ti-Tschermak
(3) $^{VI}R^{2+}$ + 2$(OH)^- \leftrightarrow {}^{VI}Ti^{4+}$ + 2O^{2-} + H_2, known as Ti-oxy or as deprotonation mechanism (Dyar *et al.,* 1993)

while the most common mechanisms involving Fe^{3+} are:

(1) 3 $^{VI}R^{2+} \leftrightarrow 2{}^{VI}Fe^{3+} + {}^{VI}\square$, known as Fe^{3+}-vacancy substitution
(2) $^{VI}R^{2+}$ + $^{IV}Si^{4+} \leftrightarrow {}^{VI}Fe^{3+}$ + $^{IV}Al^{3+}$, known as Fe^{3+}-Tschermak
(3) $^{VI}R^{2+}$ + $OH^- \leftrightarrow {}^{VI}Fe^{3+}$ + O^{2-} + ½ H_2, known as Fe^{3+}-oxy-substitution
(4) $^{VI}R^{2+}$ + $K^+ \leftrightarrow {}^{VI}Fe^{3+}$ + $^{VI}\square$, known as exfoliation by loss of interlayer K.

The calculation of the crystal chemical formulae given in Table 2 was initially performed by combining EMPA, C-H-N and Mössbauer data. Crystal-chemical formulae were obtained: 1) using as basis 12 (O, OH, F, Cl); 2) considering the oxidation state and the structural role of Fe as valued by Mössbauer spectroscopy; 3) assuming all Ti as Ti^{4+}. From Table 2 it can be noted that five cations (Al, Mg, Fe, Ti, Mn) populate the octahedral sheet and that their sum is very close to full occupancy. The final formulae were obtained allowing H_2O variation within 1σ, and the final populations, given in Table 9, were obtained from a least-squares minimization procedure combining chemical analysis, spectroscopic data and the results from the structure refinement. The best agreement was observed when all Ti was located at M2 together with Fe^{3+} and Al to fill this site. The anion radius used here was calculated according to Kogarko *et al*. (2005). The mean <M-O> distances estimated on the basis of the EMPA-derived molar fractions show a satisfactory agreement when compared with those obtained from X-ray refinement (Table 7); moreover, a good agreement is found when comparing the mean atomic numbers derived from the structure refinements and those calculated from crystal-chemical formulae (Table 7). We note that additional arguments, described above, support the oxy-substitution and other structural mechanisms when Ti and Fe^{3+} are introduced into the structure, like the shift of the M2 cation toward the O(4) oxygen.

Table 10. Band position (cm^{-1}), width (cm^{-1}), normalized relative intensity and assignment for the bands of Fig. 4.

Band	Position	Width	Rel. Int.	Assignment
A	3706	26.4	0.37	MgMgMg-OH- ^{A}K-OH
B	3685	26.6	0.23	MgMgMg-OH- ^{A}K-O^{2-}
C	3663	28.3	0.23	MgMgFe^{3+}-OH- ^{A}K-OH
D	3641	31.0	0.13	MgMgFe^{3+}-OH- ^{A}K-O^{2}
E	3609	37.4	0.04	–

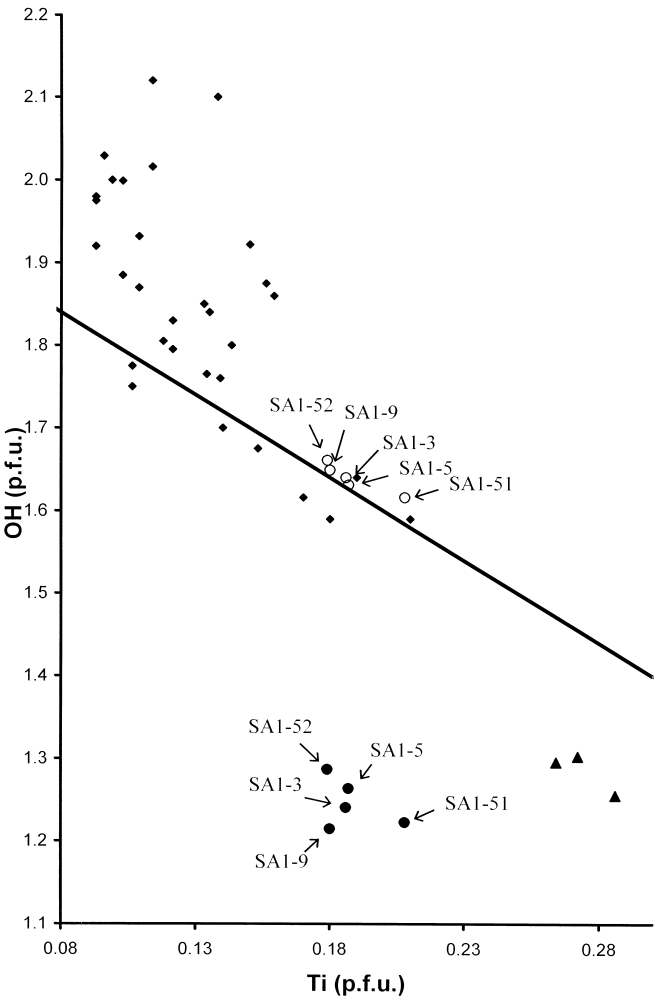

Fig. 5. OH *vs*. Ti. Solid line represents the ideal model of Ti-oxy substitution.
Filled circles = this work; open circles = our samples in case of only Ti-oxy substitution; diamonds = data from Dyar *et al*. (1993); triangles = data from Cesare *et al*. (2003).

The composition of Mt. Vulture SA1 samples falls outside the OH *vs*. Ti plot (Fig. 5, the labelled specimens below the straight line) of Cesare *et al*. (2003). This misfit is explained considering that in the micas examined here there are cations other than Ti, *i.e*. (Fe^{3+} + Al) which are involved in the oxy-substitution mechanisms and are not considered in the plot of Fig. 5. As an example let us consider the SA1-3 specimen. The expected OH content, considering the Ti-oxy substitution only, is ~0.35 a.p.f.u. However, this sample has minor but significant F substituting for OH (0.10 a.pf.u.) and 0.25 a.pf.u. (Fe^{3+} + Al) participating to the oxy-substitution (Table 9). Therefore, excluding OH contribute for F↔OH replacement, plots of OH *vs*. Ti + (Fe^{3+}, Al^{3+}) oxy-substitution would produce a better fitting as shown in Fig. 5 (the labelled specimens above the straight line).

In conclusion, the deprotonation mechanism needed to balance the excess of positive charge involves 0.659 OH group. This results is in good agreement with the indication of crystal-chemical formula, *i.e*. 0.654 OH^-, and supports the starting hypothesis that titanium is present in the structure only as Ti^{4+}. Accordingly, one possible scheme involving the main substitution mechanisms working in the structure is shown below:

(a) $^{VI}Fe^{3+} + {}^{IV}Al^{3+} \leftrightarrow {}^{VI}Mg^{2+} + {}^{IV}Si^{4+}$ (0.273 a.p.f.u.)
(b) $^{VI}Fe^{3+} + O^{2-} \leftrightarrow {}^{VI}Mg^{2+} + OH^-$ (0.092 a.p.f.u.)
(c) $^{IV}Al^{3+} + O^{2-} \leftrightarrow {}^{VI}Mg^{2+} + OH^-$ (0.170 a.p.f.u.)
(d) $^{VI}Ti^{4+} + 2O^{2-} \leftrightarrow {}^{VI}Mg^{2+} + 2OH^-$ (0.186 a.p.f.u.)
(e) $^{XII}Ba + O^{2-} \leftrightarrow K + OH^-$ (0.025 a.p.f.u.).

Acknowledgements: The authors are grateful to Mr. Marcello Serracino for assistance during electron-probe microanalyses at the Centro di Studio per il Quaternario e l'Evoluzione Ambientale, CNR, Rome. We thank Dr. A. Giaretta for C-H-N measurements at CNR-IGC, Padova. This work was supported by the COFIN-MIUR (2004).

References

Betteridge, P. W., Carruthers, J. R., Cooper, R. I., Prout, K., Watkin, D.J. (2003): Crystals version 12: software for guided crystal structure analysis. *J. Appl. Cryst.*, **36**, 1487.

Brigatti, M.F. & Guggenheim, S. (2002): Mica crystal chemistry and the influence of pressure, temperature, and solid solution on atomistic models. *Rev. Mineral. Geochem.*, **46**, 1-97.

Brigatti, M.F., Galli, E., Poppi, L. (1991): Effect of Ti substitution in biotite-1*M* crystal chemistry. *Am. Mineral.*, **76**, 1174-1183.

Brigatti, M.F., Caprilli, E., Marchesini, M., Poppi, L. (2003): The crystal structure of roscoelite-1*M*. *Clays Clay Minerals,* **51**, 301-308.

Bruker (2001): *SAINT*. Bruker AXS Inc., Madison, Wisconsin, USA.

– (2003): *APEX2*. Bruker AXS Inc., Madison, Wisconsin, USA.

Caggianelli, A., De Fino, M., La Volpe, L., Piccarreta, G. (1990): Mineral chemistry of Monte Vulture Volcanics: petrological implications. *Mineral. Petrol.*, **41**, 215-227.

Cesare, B., Cruciani, G., Russo, U. (2003): Hydrogen deficiency in Ti-rich biotite from anatectic metapelites (El Joyazo, SE Spain): Crystal-chemical aspects and implications for high-temperature petrogenesis. *Am. Mineral.*, **88**, 583-595.

Cruciani, G. & Zanazzi, P.F. (1994): Cation partitioning and substitution mechanism in 1*M* phlogopite: A crystal chemical study. *Am. Mineral.*, **79**, 289-301.

Della Ventura, G., Robert, J.L., Hawthorne, F.C. (1996): Infrared spectroscopy of synthetic (Ni,Mg,Co)-potassium-richterite. *In* M.D. Dyar, C. McCammon, M.W. Schaefer, Eds., Mineral Spectroscopy: a Tribute to Roger G. Burns, p. 55-63. The Geochemical Society Special Publication No. **5**.

Donnay, G., Donnay, J.D.H., Takeda, H. (1964a): Trioctahedral one-layer micas. II Prediction of the structure from composition and cell dimensions. *Acta Cryst.*, **17**, 1374-1381.

Donnay, G., Morimoto, N., Takeda, H., Donnay, J.D.H. (1964b): Trioctahedral onelayer micas. I. Crystal structure of a synthetic iron mica. *Acta Cryst.*, **17**, 1369-1373.

Dyar, M.D., Guidotti, C.V., Holdaway, M.J., Colucci, M. (1993): Nonstoichiometric hydrogen contents in common rock-forming hydroxyl silicates. *Geochim. Cosmochim. Acta*, **57**, 2913-2918.

Foley, S.F. (1989): Experimental constraints on phlogopite chemistry in lamproites: 1. The effect of water activity and oxygen fugacity. *Eur. J. Mineral.*, **1**, 411-426.

Guggenheim, S. & Frimmel, H.E. (1999): Ferrokinoshitalite, a new species of brittle mica from the Broken Hill mine, South Africa:

Structural and mineralogical characterization. *Can. Mineral.*, **37**, 1445-1452.

Güven, N. (1971): The crystal structure of 2*M*1 phengite and 2*M*1 muscovite. *Z. Kristallogr.,* **134**, 196-212.

Hawthorne, F.C., Ungaretti, L., Oberti, R. (1995): Site populations in minerals: terminology and presentation of results. *Can. Mineral.*, **33**, 907-911.

Hazen, R.M. & Burnham, C.W. (1973): The crystal structure of one layer phlogopite and annite. *Am. Mineral.*, **58**, 889-900.

Johnston, C.T., Agnew, S.F., Bish, D.L. (1990): Polarized single-crystal Fourier-transform infrared microscopy of Ouray dickite and Keokuk kaolinite. *Clays Clay Minerals*, **38**, 573-583.

Kogarko, L.N., Uvarova, Y.A., Sokolova, E., Hawthorne, F.C., Ottolini, L., Grice, J.D. (2005) Oxykinoshitalite, a new species of mica from Fernando-de-Norohna Island, Pernambuco, Brazil: occurrence and crystal structure. *Can. Mineral.*, **43**, 1501-1510.

Lagarec, K. & Rancourt, D.G. (1998): RECOIL. Mössbauer spectral analysis software. Department of Physics, University of Ottawa, Ottawa, Canada.

Libowitzky, E. & Rossman, G.R. (1996): Principles of quantitative absorbance measurements in crystals. *Phys. Chem. Minerals*, **23**, 319-327.

Mesto, E., Schingaro, E., Scordari, F., Ottolini L. (2006): Electron microprobe analysis, secondary ion mass spectrometry and single crystal X-ray diffraction study of phlogopites from Mt. Vulture, Potenza, Italy: Consideration of cation partitioning. *Am. Mineral.*, **91**, 182-190.

Pouchou, J.L. & Pichoir, F. (1985): 'PAP' $\Phi(\rho Z)$ procedure for improved quantitative micro-analysis. *Microbeam Analysis*, 104-160.

Rancourt, D.G. (1994a): Mössbauer Spectroscopy of Minerals I. Inadequacy of Lorentzian line doublets in fitting spectra arising from Quadrupole Splitting Distributions. *Phys. Chem. Minerals*, **21**, 244-249.

— (1994b): Mössbauer Spectroscopy of Minerals II. Problems of resolving cis and trans octahedral Fe^{2+} sites. *Phys. Chem. Minerals*, **21**, 250-257.

Rancourt, D.G. & Ping, J.Y. (1991): Voigt-based methods for arbitrary-shape static hyperfine parameter distributions in Mössbauer spectroscopy. *Nucl. Instrum. Meth. Phys. Res.*, **B58**, 85-97.

Rancourt, D.G., Ping, J.Y., Berman, R.G. (1994): Mössbauer Spectroscopy of Minerals III. Octahedral-site Fe^{2+} Quadrupole Splitting Distributions in the phlogopite-annite series *Phys. Chem. Minerals*, **21**, 258-267.

Redhammer, G.J., Beran, A. , Schneider, J., Amthauer, G., Lottermoser W. (2000): Spectroscopic and structural properties of synthetic micas on the annite-siderophyllite binary: Synthesis, crystal structure refinement, Mössbauer, and infrared spectroscopy. *Am. Mineral.,* **85**, 449–465.

Renner, B. & Lehmann, G. (1986): Correlation of angular and bond length distortions in TO_4 units in crystals. *Z. Kristallogr.*, **175**, 43-59.

Rieder, M., Cavazzini, G., D'Yakonov, Y.S., Frank-Kamenetskii, V.A., Gottardi, G., Guggenheim, S., Koval, P.V., Müller, G., Neiva, A.M.R., Radoslovich, E.W., Robert, J.-L., Sassi, F.P., Takeda, H., Weiss, Z., Wones, D.R. (1998): Nomenclature of micas. *Can. Mineral.*, **36**, 905-912.

Righter, K., Dyar, M.D., Delaney, J.S., Vennemann, T.W., Hervig, R.L., King, P.L. (2002): Correlations of octahedral cations with OH^-, O^{2-}, Cl^-, and F^- in biotite from volcanic rocks and xenoliths. *Am. Mineral.*, **87**, 142-153.

Robert, J.-L., Della Ventura, G., Hawthorne, F.C. (1999): Near-infrared study of short-range disorder of OH and F in monoclinic amphiboles. *Am. Mineral.*, **84**, 86-91.

Robinson, K., Gibbs, G.V., Ribbe, P.H. (1971): Quadratic elongation, a quantitative measure of distortion in coordination polyhedra. *Science*, **172**, 567-570.

Schingaro, E., Scordari, F., Ventruti, G. (2001): Trioctahedral micas-1*M* from Mt.Vulture (Italy): Structural disorder and crystal chemistry. *Eur. J. Mineral.*, **13**, 1057-1069.

Schingaro E., Mesto E., Scordari F., Brigatti, M.F., Pedrazzi, G. (2005): Cation site partitioning in Ti-rich micas from Black Hill (Australia): a multi-technical approach. *Clays Clay Minerals,* **53**, 179-189.

Scordari, F., Schingaro, E., Pedrazzi, G. (1999): Crystal chemistry of melanites from Mt. Vulture (Southern Italy). *Eur. J. Mineral.*, **11**, 855-869.

Serratosa, J.M. & Bradley, W.F. (1962): Determination of the orientation of OH bond axes in layer silicates by infrared absorption. *J. Phys. Chem.*, **62**, 1164-1167.

Shannon, R.D. (1976): Revised effective ionic radii and systematic studies of interatomic distances in halides and chalcogenides. *Acta Cryst.*, **A32**, 751-767.

Sheldrick, G.M. (2003): *SADABS*. University of Göttingen, Germany.

Strens, R.S.J. (1974): The common chain, ribbon and ring silicates. *In* V.C. Farmer, eds. The Infrared Spectra of Minerals. *Mineral. Soc. Monogr.*, **4**, 305-330.

Toraya, H. (1981): Distortions of octahedra and octahedral sheets in 1*M* micas and the relation to their stability. *Z. Kristallogr.*, **157**, 173-190.

Turrell, G. (1972): Infrared and Raman spectra of minerals. Academic Press, London.

Tyrna, P.L. & Guggenheim, S. (1991): The crystal structure of norrishite, $KLiMn_2^{3+}Si_4O_{12}$: An oxygen-rich mica. *Am. Mineral.*, **76**, 266-271.

Vedder, W. & McDonald, R.S. (1963): Vibration of the OH ions in muscovite. *J. Chem. Phys.,* **38**, 1583-1590.

Virgo, D. & Popp, R.K. (2000): Hydrogen deficiency in mantle-derived phlogopites. *Am. Mineral.*, **85**, 753-759.

Waters, D.J. & Charnley, N.R. (2002): Local equilibrium in polymetamorphic gneiss and the titanium substitution in biotite. *Am. Mineral.*, **87**, 383-396.

Weiss, Z., Rieder, M., Chmielovà, M., Krajìcek, J. (1985): Geometry of the octahedral coordination in micas: a review of refined structures. *Am. Mineral.*, **70**, 747-757.

Received 23 May 2005
Modified version received 14 November 2005
Accepted 29 March 2006